FERMILAB-PUB-78-117-E

E-4

UM HE 78-30
August, 1978

RECEIVED
OCT 3 0 1978
DIRECTORS OFFICE
FERMILAB

Neutron-Proton Differential Cross Sections at Fermilab Energies*

C.E. DeHaven, Jr.†, C.A. Ayre‡, H.R. Gustafson, L.W. Jones
M.J. Longo, P.V. Ramana Murthy§, T.J. Roberts, M.R. Whalley

Randall Laboratory of Physics
University of Michigan
Ann Arbor, MI 48109

ABSTRACT

We report the results of an experiment which measured n-p elastic scattering differential cross sections over a range in -t from 0.15 to ~ 3.6 $(GeV/c)^2$ for incident neutron momenta from 70 to 400 GeV/c. We find the logarithmic slope parameter, evaluated at $-t = 0.2\ (GeV/c)^2$, to be consistent with existing proton-proton parameterizations. The data exhibit a dip in the cross section near -t 1.4 $(GeV/c)^2$ for incident neutron momenta above 200 GeV/c. For neutron momenta less than 280 GeV/c, the neutron-proton cross sections are found to be higher than existing proton-proton data in the range $0.7 \le -t \le 1.3\ (GeV/c)^2$ which is in contradiction to most Regge predictions.

*Work supported by the National Science Foundation

†Present Address: Bell Telephone Laboratory, Whippany, NJ, USA

‡Present Address: Department of Physics, University of Durham Durham, England

§Permanent Address: Tata Institute for Fundamental Research, Bombay, India

I. INTRODUCTION

We describe here an experiment to measure neutron-proton elastic scattering differential cross sections. A brief report has already been published (1). A more detailed description of the experimental techniques can be found in Refs. 2 and 3. Cross sections were measured in the momentum range 70 to 400 GeV/c with an incident neutron beam at Fermi National Accelerator Laboratory. Four-momentum transfers squared from 0.15 to ~ 3.6 $(\mathrm{GeV/c})^2$ were covered. Cross sections for n-p charge exchange scattering have already been measured in this momentum range (4). There is also considerable data on p-p elastic scattering (5,6). The p-p data at 200 GeV/c and above show an interesting dip near $|t| = 1.4$ $(\mathrm{GeV/c})^2$ and a second maximum at larger $|t|$. One of the objectives of this experiment was to determine if the n-p cross sections show a similar behavior.

The organization of this paper is as follows: In Section II, a description of the apparatus is presented. Section III details the event reconstruction techniques and the calculation of the cross sections. The results are presented in Section IV in graphic and tabular form. In addtion, various parameterizations are presented and the data are compared to existing p-p data. We summarize our results in Section V.

II. EXPERIMENTAL APPARATUS

A schematic diagram of the experiment is shown in Figure 1. The neutron beam was incident upon a liquid hydrogen target, 30.5 cm long and 5.1 cm diameter. The spot size of the beam varied from 2 mm wide x 3 mm high to 30 x 50 mm, depending on the desired intensity. The beam intensity ranged from $\sim 10^5$ neutrons per 1 sec spill at the low $|t|$ settings to $\sim 2 \times 10^7$ for the large $|t|$ data. Charged particles were removed from the beam by sweeping magnets. Photons were effectively removed by two lead filters with a total thickness of approx. 11 rad. lengths. For neutron momenta of approx. 100 GeV/c, the K_L°/n ratio is $\approx .05$; above 150 GeV/c it is $\leqslant .01$. The $\bar{n}$ contamination is negligible.

The recoil proton momentum and scattering angle were measured by a spectrometer consisting of four wire spark chamber modules SC1-SC4, each with X-Y-U-V magnetostrictive readout planes, and a 105 cm x 100 cm analyzing magnet with a 15.1 cm gap. The strength of the magnetic field was 7.6 kG for the low $|t|$ data $(0.8 \leqslant |t| \leqslant 1.0\ (\mathrm{GeV/c})^2)$ and 12.5 kG for the high $|t|$ data $(0.8 \leqslant |t| \leqslant 3.6\ (\mathrm{GeV/c})^2$. Part of the trigger requirement was a fast coincidence between scintillation counters P_1, P_2 and P_3 which indicated that a charged particle had traversed the spectrometer. The scattered neutron was required to interact in a neutral particle detector and produce a charged particle shower. The detector contained 30 wire spark chambers, 28 zinc plates and six scintillation counters (see inset of Fig. 1) and was placed 71 m downstream of the hydrogen target. We determined the interaction point to an accuracy ~2 mm FWHM by locating the vertex of the charged particle shower in the chambers. The neutron scattering angle was then defined by the interaction point in the neutral particle detector and a point on the proton trajectory within the illuminated part of the liquid hydrogen target. The second part of the triggering requirement was a fast coincidence between any two of the six scintillation counters indicating that at least one charged particle had passed through the neutron detector. Veto counters $A_1, \ldots A_6$, not all of which are shown in Figure 1, were used to reduce the trigger rate from inelastic events. These almost completely surrounded the target except on the recoil proton side. All except A_6 consisted of lead-scintillator sandwiches with approx. 3 rad. lengths of lead, so that they were sensitive to photons from π° decays. The veto counters typically reduced the trigger rate a factor of 50. A counter telescope M and a total absorption calorimeter were used to monitor the beam flux.

III. DATA ANALYSIS

The differential cross sections were computed by reconstructing the event from the raw data which had been written on magnetic tape by the online computer. This was accomplished by first computing the recoil proton momentum and scattering angle from the charged particle spectrometer data. The neutron scattering angle was then determined by extracting the shower vertex from the neutral particle detector data. This point and a point in the LH_2 target on the proton trajectory defined the scattering angle. Thus, all kinematic variables were measured except for the momenta of the incident and scattered neutrons. Momentum and energy conservation allowed a two-constraint fit to the hypothesis of n-p elastic scattering. The fitting program calculated the unmeasured momenta and a χ^2 for the fit. Events with $\chi^2 < 10$ were considered to be elastic and were binned according to the incident neutron momentum and the four-momentum transfer squared, t. In Figure 2, χ^2 distributions are shown for a low $|t|$ range where the background is expected to be small and for the dip region $1.8 \leq -t \leq 3.0$ $(GeV/c)^2$ where the background is expected to be more significant. The smooth curves show the expected distributions for a two-constraint fit to a sample of elastic events. The distributions are dominated by inelastic events for $\chi^2 \geqslant 8$.

Various corrections have been applied to the data. We have calculated the geometric acceptance by a Monte Carlo technique which was checked using an approx. analytic method. Two positions of the detectors were used to cover the desired $|t|$ range. Figure 3 shows the variation of the geometric acceptance with t for incident momenta of 100 and 200 GeV/c for the two positions.

Inelastic background corrections, as estimated from the χ^2 distributions, amounted to less than 3% at small $|t|$ and less than 35% at large $|t|$. Corrections for nuclear absorption of the recoil proton ranged from 2 to 4%. Target empty corrections were negligible. It is important to note that the neutron detection efficiency, which was about 65%, does not significantly affect the t-dependence of the measured cross sections because the energy of the scattered neutron differs from that of the incident neutron by at most 2%.

We have estimated the uncertainties in the calculated incident momentum P and the measured value of the four-momentum transfer squared t. This was accomplished by examining the fitted errors in the neutron and proton scattering angles and the proton momentum as determined by the kinematic reconstruction program.

In Figure 4a, the uncertainty in t, Δt, is plotted against t. Because the value of t is measured directly, the uncertainty in t is not dependent on the incident neutron momentum. Since multiple Coulomb scattering is responsible for a large fraction of the uncertainty in t, the error increases nearly linearly with increasing $|t|$. The fractional uncertainty is approximately constant at 1% which implies that at $|t| = 1.0$ $(GeV/c)^2$, the error in t is 0.01 $(GeV/c)^2$. Since the bins are 0.1 $(GeV/c)^2$ wide in this region, the error is only 10% of the bin width and hence does not appreciably affect the cross section measurement.

The uncertainty in the incident neutron momentum, ΔP, was dependent on both P and t. This dependence is shown in Figure 4b. In the case of small $|t|$ and large P, the error in P was nearly 40% of the bin width in P. The uncertainty in incident momentum is dependent on the horizontal width of the beam. For the small $|t|$ setting a smaller beam spot was used. The dashed line in Figure 4b shows the typical behavior of $\Delta P/P$ for the small $|t|$ setting. The solid lines in Figure 4b show the errors for the large $|t|$ setting.

The uncertainty in the incident neutron momentum smears out the neutron spectrum. Since the resolution varies with t, this effect is t dependent. Corrections for this were only significant for the highest momentum bin where they were $<4\%$.

Both low $|t|$ and high $|t|$ data were collected in each of two running periods which were spaced six months apart. In principle, it is possible to use either the telescope "M" or the total absorption calorimeter to provide relative normalization between data sets. However, because of possible shifts in the energy spectrum due to different production angles of the neutral beam for the two running periods, the data sets were normalized relative to each other by tying the data together in various overlap regions. This typically involved five data points per data set and we estimate the uncertainty in this procedure to be approximately 4%. After the data were combined, the overall normalization was calculated by fitting the data to the form $d\sigma/d|t| = Ae^{Bt+Ct^2}$ in the range $.17 \leq |t| \leq .7$ and extrapolating to $t = 0$. The intercept was then adjusted to the optical theorem point as given by

$$\frac{d\sigma(t = 0)}{d|t|} = \frac{1}{16\pi}\sigma_T^2 (1 + \rho^2). \qquad (1)$$

The values of σ_T used were calculated from a fit of n-p total cross section data given by Murthy et al.(7). If we assume that the ratio of the real to imaginary parts of the forward scattering amplitude, ρ, for n-p elastic scattering is approximately the same as that for p-p scattering(8), the contribution of the ρ^2 term in Eq. 1 is negligible. The uncertainty in the overall normalization is estimated to be $^{+5}_{-15}\%$, mainly due to the uncertainty in the extrapolation to $t = 0$.

IV. RESULTS

The differential cross sections for n-p elastic scattering as measured by this experiment are presented in Figure 5. The continuous neutron spectrum has been divided into seven momentum bins. Each data set in Figure 5 has been labeled with the nominal momentum value of that bin. The momentum ranges were chosen to provide comparable statistical accuracy for each bin, while making them narrow enough to preserve any energy-dependent effects that may exist. The width of the t bins increases as $|t|$ increases in order to partially compensate for the lower data collection rate at higher $|t|$. While bins smaller than 0.1 $(GeV/c)^2$ in the region $-t \approx 1.4$ $(GeV/c)^2$ would have been desirable, it was not possible given the number of events in that region.

Tabulations of the differential cross sections are presented in Tables I-VII. The heading of each table gives the range of incident neutron momentum for that bin (P_{LAB}), the average center-of-mass energy squared (s_{ave}), the n-p total cross section (σ_T) and the center-of-mass momentum (P^*). In the tables, t_{ave} is the average value of $|t|$ for all events in the bin, and θ^* is the center-of-mass scattering angle.

The errors plotted in Figure 5 and listed in Tables I-VII include statistical uncertainties as well as the point-to-point systematic errors. However, the uncertainty of the overall normalization of the data, estimated to be $^{+5}_{-15}\%$ for each momentum bin, has not been included in the error assignment. The point-to-point systematics reflect the uncertainties of various corrections such as geometric detection efficiency, nuclear absorption of protons, and so forth. This estimate was added in quadrature to the statistical uncertainties in the number of good events and background events to yield the final error assignments. Uncertainties due to possible K^o_L contamination in the beam at lower energies have not been included.

The following observations can be made. The data exhibit the usual diffraction peak which shrinks with increasing energy. Above 200 GeV/c, the data show the gradual evolution of a dip in the cross section near $|t| = 1.4$ $(GeV/c)^2$ as the incident neutron energy increases. While the dip is similar to that previously reported in p-p elastic scattering (5,6,9), the n-p cross sections are generally higher in this region and do not appear to vary as rapidly as a function of energy in the dip region. The cross sections then rise to a second maximum and begin to fall in a much slower fashion. As in p-p data, the logarithmic slope beyond the second maximum is ~ 2 $(GeV/c)^{-2}$.

Traditionally, elastic scattering has been characterized in the diffraction region by the logarithmic slope parameter $b^*(s,t)$ with the interpretation that the radius of the strong interaction is proportional to b^* where b^* is defined as

$$b^*(s,t) \equiv \frac{\partial}{\partial t} \{\ell n \frac{d\sigma}{dt} (s,t)\}.$$

We have fit the data to the form

$$\frac{d\sigma}{dt} = A\, e^{Bt+Ct^2}$$

in the region $.17 \leq -t \leq .67\ (GeV/c)^2$. For this parameterization, b^* is given by

$$b^*(s,t) = B(s) + 2C(s)t.$$

We have evaluated b^* at $t = -0.2\ (GeV/c)^2$. The results are shown in Figure 6, where the data from this experiment are compared to previous n-p and p-p data (3,9,10,11). The slope parameters have been plotted as a function of s, the center-of-mass energy squared. Also shown in the prediction of the Reggeized absorption model of Kane and Seidl(12). There seems to be very little difference between the n-p and p-p slope parameters over the interval $100 \leq s \leq 1000\ GeV^2$.

One of the more interesting areas of comparison between n-p and p-p data is in the region $-t \approx 1.4\ (GeV/c)^2$. Given the dip in p-p data, it is of interest to look for similar structure in the n-p data and to see if it sevelops in the same manner. In Figure 7 we compare our data at 200 GeV/c with the p-p data of Akerlof <u>et al</u>.(6) and to the preliminary data of Bomberowitz <u>et al</u>.(13).

As discussed earlier, the development of the dip in n-p scattering seems to be less dramatic than in p-p scattering. Whereas only a shoulder exists in the n-p data at 200 GeV/c, a rather pronounced dip occurs in the p-p data. The n-p data appear to be higher in the dip region, but given the rather large errors in both the p-p and n-p data it is not possible to draw strong conclusions.

While examination of the dip region does not lead to any definite conclusions, some interesting comparisons can be made in the region $0.6 \leq -t \leq 1.2$ $(GeV/c)^2$. In Figure 8, the n-p data are compared to the p-p elastic scattering data of Akerlof _et al_., Bomberowitz _et al_., and Kwak _et al_.,(4) in the range $0.70 \leq -t \leq 1.50$ $(GeV/c)^2$. At 100 GeV/c, the n-p and p-p cross sections are comparable up to $-t \approx 0.8$. At larger $|t|$, they begin to diverge with the n-p cross section approximately 3 times the p-p cross section near $-t \approx 1.25$ $(GeV/c)^2$. This difference persists out to $-t \approx 1.4$ $(GeV/c)^2$. At 200 GeV/c the cross sections remain comparable out to $-t \approx 0.95$ $(GeV/c)^2$, beyond which they begin to differ. As in the 100 GeV/c data, the n-p data is approx. three times the p-p data at $-t \approx 1.25$ $(GeV/c)^2$. [In order to see if the n-p data exhibit a strong energy dependence, we have also binned the data for the incident momentum range 200 to 240 GeV/c. The cross sections remain unchanged out to $-t \approx 1.3$ $(GeV/c)^2$.]

The cross sections at 280 GeV/c agree out to $-t \approx 1.2$ $(GeV/c)^2$. Thus, as the incident momentum increases, the n-p and p-p cross sections agree out to larger values of t. In Regge theory the difference between n-p and p-p elastic scattering is caused by a difference in the sign of the ρ and A_2 isovector amplitudes. The magnitude of these Reggeon amplitudes should decrease with increasing energy. The comparison of the n-p data with existing p-p data indicate just such an effect. From this comparison, the contribution of the ρ and A_2 above 280 GeV/c would seem to be small, at least for $t \leq 1.4\ (\mathrm{GeV/c})^2$. However, in simple Regge models, the n-p cross sections are expected to be <u>less</u> than or equal to the p-p cross sections. The comparison of the n-p cross sections measured by this experiment with existing p-p data indicate the opposite effect. In Figure 9, the difference $(d\sigma/dt)_{np} - (d\sigma/dt)_{pp}$ is plotted against s at fixed t. Although there are only three data points, they are approximated by a straight line with slope $\sim(-2)$. One example of a mechanism which could account for greater n-p cross sections would be the interference between the f_o and the A_2 net helicity flip amplitudes(15). If an interference term between the f_o and A_2 is responsible for the greater n-p cross sections, then it should go like

$$\frac{d\sigma}{dt}\Big|_{np} - \frac{d\sigma}{dt}\Big|_{pp} \propto s^{2\alpha(t)-2}$$

where $\alpha(t) \cong 0.4 - 0.85\ |t|$. For $-t = 1.25\ (\mathrm{GeV/c})^2$, this corresponds to a power in s ~ -3.3. If, on the other hand, an interference term between the Pomeron and an isovector were responsible, the difference should go like $s^{\alpha(t)-1}$ or $s^{-1.7}$. Although the data would seem to favor a Pomeron-Reggeon interference term, the data are inadequate to distinguish clearly between Pomeron-Reggeon and Reggeon-Reggeon interference terms.

V. SUMMARY

Differential cross sections for neutron-proton elastic scattering have been measured over the incident neutron momentum range to 70 to 400 GeV/c. The results can be summarized as follows:

1. At $-t = 0.2\ (\text{GeV/c})^2$, the n-p logarithmic slope parameters agree with existing p-p data for $s \leqslant 1000\ \text{GeV}^2$.
2. In the region $0.8 \leq -t \leq 1.2\ (\text{GeV/c})^2$ for incident momenta less than 280 GeV/c, n-p cross sections are significantly higher then the p-p cross sections which indicates that net helicity-flip amplitudes may be important in this region.
3. As the incident momentum increases, better agreement is reached between the n-p and p-p cross sections, in qualitative agreement with Regge theory.
4. A dip in the n-p cross section above 200 GeV/c has been confirmed although the detailed behavior seems to be different from that of the p-p data.

A synopsis of neutron-proton elastic scattering over a large momentum range is presented in Figure 10 where some representative n-p elastic scattering data have been plotted against $|t|$ over a large energy range. (The numbers after the references in parentheses give the incident momentum.) If we fix $-t = 2.0\ (\text{GeV/c})^2$, the scattering angles in the c.m.s. go from $\theta_{cms} \sim 40°$ at low momenta to $\theta_{cms} \sim 8°$ at Fermilab energies. The lower momenta cross sections(3) at this $|t|$ drop like s^{-n} where $n \sim 8 - 10$. By Fermilab energies, the cross sections at $-t = 2$ show little change between 100 and 360 GeV/c.

We wish to express our appreciation to the entire Fermilab staff for their support of this experiment. We also wish to thank Jim Stone, John Chanowski, Geoff Mills and Bill Larsen for their help during various phases of the experiment. Useful discussions with Gordon Kane and Andy Seidl are gratefully acknowledged.

<u>REFERENCES</u>

1. C.E. DeHaven <u>et al.</u>, to be published in Phys. Rev. Letters.
2. C.E. DeHaven Jr., Ph.D. Thesis, University of Michigan (Physics), 1978.
3. J.L. Stone <u>et al.</u>, to be published in Nucl. Physics B;
   J.L. Stone, Ph.D. Thesis, University of Michigan (Physics), 1977.
4. H. Barton <u>et al.</u>, Phys. Rev. Lett. <u>37</u>, 1656 (1976).
5. A. Bohm <u>et al.</u>, Phys. Lett. <u>49B</u>, 491 (1974).
6. C. Akerlof <u>et al.</u>, Phys. Lett. <u>59B</u>, 197 (1975).
7. P.V.R. Murthy <u>et al.</u>, Nucl. Phys. <u>B92</u>, 269 (1975).
8. V. Bartenev <u>et al.</u>, Phys. Rev. Lett. <u>31</u>, 1367 (1973).
9. V. Böhmer <u>et al.</u>, Nucl. Phys. <u>B91</u>, 266 (1975).
10. G. Barbiellini <u>et al.</u>, Phys. Lett. <u>39B</u>, 663 (1972).
11. D.S. Ayres <u>et al.</u>, Phys. Rev. Lett. <u>35</u>, 1195 (1975).
12. G.L. Kane and A. Seidl, Rev. Mod. Phys. <u>48</u>, 309 (1976).
13. R. Bomberowitz, Ph.D. Thesis, Rutgers University (Physics) 1977;
    R. Bomberowitz <u>et al.</u>, Bull. Am. Phys. Soc. <u>23</u>, 52 (1978).
14. N. Kwak <u>et al.</u>, Phys. Lett. <u>58B</u>, 233 (1975).
15. G. Kane, private communication.

TABLE I. P_{LAB} = 70-125 GeV/c, s_{ave} = 189(GeV/c)^2

(σ_T = 38.8 mb, P* = 6.82 GeV/c)

t_{ave}	dσ/dt mb/(GeV/c)^2	Error	θ* deg.
.152	.191E+02	.97E+00	3.278
.175	.141E+02	.63E+00	3.517
.205	.999E+01	.45E+00	3.807
.238	.743E+01	.34E+00	4.105
.279	.475E+01	.22E+00	4.441
.323	.313E+01	.15E+00	4.779
.373	.208E+01	.11E+00	5.132
.423	.120E+01	.72E-01	5.469
.473	.822E+00	.55E-01	5.787
.521	.474E+00	.38E-01	6.073
.576	.270E+00	.13E-01	6.381
.625	.170E+00	.83E-02	6.648
.674	.111E+00	.56E-02	6.905
.723	.709E-01	.38E-02	7.152
.773	.500E-01	.28E-02	7.396
.824	.327E-01	.20E-02	7.636
.874	.199E-01	.14E-02	7.865
.924	.142E-01	.11E-02	8.087
.972	.897E-02	.78E-03	8.295
1.043	.547E-02	.44E-03	8.593
1.150	.241E-02	.28E-03	9.024
1.247	.102E-02	.18E-03	9.397
1.346	.654E-03	.15E-03	9.764
1.449	.639E-03	.16E-03	10.132
1.539	.140E-03	.71E-04	10.443
1.649	.260E-03	.12E-03	10.810
1.756	.839E-04	.50E-04	11.157
1.957	.114E-03	.64E-04	11.780
2.093	.994E-04	.58E-04	12.184

TABLE II. P_{LAB} = 125-175 GeV/c, s_{ave} = 283 GeV^2

(σ_T = 39.1 mb, P* = 8.36 GeV/c)

t_{ave}	dσ/dt mb/(GeV/c)^2	Error	θ* deg.
.152	.182E+02	.87E+00	2.672
.174	.129E+02	.56E+00	2.862
.204	.922E+01	.41E+00	3.098
.239	.675E+01	.30E+00	3.351
.279	.454E+01	.21E+00	3.623
.323	.302E+01	.14E+00	3.895
.373	.173E+01	.87E-01	4.186
.422	.100E+01	.56E-01	4.455
.473	.605E+00	.39E-01	4.714
.524	.409E+00	.30E-01	4.964
.576	.276E+00	.13E-01	5.201
.625	.153E+00	.73E-02	5.419
.674	.992E-01	.48E-02	5.628
.724	.664E-01	.34E-02	5.833
.774	.414E-01	.23E-02	6.032
.825	.269E-01	.16E-02	6.227
.873	.171E-01	.11E-02	6.406
.924	.112E-01	.81E-03	6.591
.972	.768E-02	.62E-03	6.760
1.041	.423E-02	.33E-03	6.996
1.144	.169E-02	.18E-03	7.334
1.245	.782E-03	.12E-03	7.652
1.345	.403E-03	.89E-04	7.954
1.451	.298E-03	.80E-04	8.262
1.552	.229E-03	.68E-04	8.545
1.662	.652E-04	.40E-04	8.843
1.758	.107E-03	.36E-04	9.095
1.921	.146E-03	.43E-04	9.509
2.124	.101E-03	.33E-04	10.000
2.278	.401E-04	.18E-04	10.357
2.567	.225E-04	.10E-04	10.996
2.986	.106E-04	.67E-05	11.862
3.404	.183E-04	.10E-04	12.669

TABLE III. P_{LAB} = 175-225 GeV/c, s_{ave} = 377 GeV^2

(σ_T = 39.5 mb, P* = 9.66 GeV/c)

t_{ave}	dσ/dt	Error	θ*
	mb/$(GeV/c)^2$		deg.
.152	.159E+02	.73 E+00	2.312
.174	.119E+02	.51 E+00	2.476
.204	.870E+01	.37 E+00	2.681
.239	.613E+01	.26E+00	2.899
.279	.398E+01	.18E+00	3.133
.323	.256E+01	.12E+00	3.371
.373	.155E+01	.74 E-01	3.622
.423	.863E+00	.46 E-01	3.857
.474	.572E+00	.33 E-01	4.083
.524	.383E+00	.25 E-01	4.293
.576	.237E+00	.11E-01	4.500
.625	.145E+00	.66 E-02	4.689
.674	.878E-01	.41 E-02	4.870
.723	.584E-01	.28 E-02	5.044
.773	.363E-01	.19 E-02	5.215
.823	.239E-01	.13E-02	5.381
.873	.154E-01	.92E-03	5.543
.923	.898E-02	.61 E-03	5.699
.974	.613E-02	.46 E-03	5.855
1.039	.281E-02	.22 E-03	6.047
1.147	.127E-02	.13E-03	6.354
1.242	.416E-03	.74E-04	6.612
1.345	.227E-03	.58E-04	6.881
1.426	.747E-04	.36E-04	7.086
1.530	.410E-04	.26E-04	7.340
1.644	.828E-04	.38E-04	7.609
1.768	.582E-04	.23E-04	7.891
1.919	.658E-04	.23E-04	8.222
2.121	.769E-04	.21E-04	8.644
2.291	.447E-04	.16E-04	8.985
2.560	.239E-04	.81E-05	9.499
2.975	.850E-05	.46E-05	10.242
3.401	.286E-05	.22E-05	10.952

TABLE IV. P_{LAB} = 225-265 GeV/c, s_{ave} = 461 GeV^2
(σ_T = 39.7 mb, P^* = 10.7 GeV/c)

t_{ave}	dσ/dt mb/$(GeV/c)^2$	Error	θ^* deg.
.151	.179E+02	.82E+00	2.081
.174	.135E+02	.57E+00	2.236
.204	.960E+01	.41E+00	2.421
.239	.666E+01	.29E+00	2.618
.279	.446E+01	.20E+00	2.829
.323	.275E+01	.12E+00	3.044
.373	.175E+01	.83E-01	3.271
.423	.996E+00	.52E-01	3.486
.473	.665E+00	.38E-01	3.685
.524	.387E+00	.26E-01	3.878
.575	.229E+00	.10E-01	4.062
.625	.134E+00	.61E-02	4.235
.674	.835E-01	.39E-02	4.398
.723	.530E-01	.26E-02	4.555
.774	.335E-01	.17E-02	4.713
.824	.193E-01	.11E-02	4.863
.873	.121E-01	.75E-03	5.005
.924	.801E-02	.55E-03	5.150
.975	.511E-02	.39E-03	5.290
1.045	.250E-02	.19E-03	5.477
1.147	.884E-03	.10E-03	5.738
1.242	.345E-03	.64E-04	5.971
1.349	.113E-03	.37E-04	6.223
1.446	.712E-04	.32E-04	6.443
1.552	.378E-04	.25E-04	6.675
1.649	.195E-04	.19E-04	6.881
1.759	.341E-04	.18E-04	7.107
1.914	.765E-04	.23E-04	7.414
2.108	.291E-04	.12E-04	7.781
2.309	.371E-04	.13E-04	8.145
2.507	.241E-04	.75E-05	8.487
2.983	.955E-05	.46E-05	9.259
3.606	.151E-05	.16E-05	10.183

TABLE V. P_{LAB} = 265-300 GeV/c, s_{ave} = 527 GeV^2

(σ_T = 39.9 mb, P* = 11.4 GeV/c)

t_{ave}	dσ/dt	Error	θ*
	mb/$(GeV/c)^2$		deg.
.151	.156E+02	.71E+00	1.946
.174	.116E+02	.49E+00	2.092
.204	.821E+01	.35E+00	2.265
.239	.551E+01	.24E+00	2.449
.279	.360E+01	.16E+00	2.646
.323	.241E+01	.11E+00	2.847
.373	.134E+01	.65E-01	3.061
.423	.815E+00	.43E-01	3.258
.474	.528E+00	.31E-01	3.449
.522	.282E+00	.20E-01	3.621
.575	.195E+00	.87E-02	3.799
.625	.116E+00	.53E-02	3.960
.674	.743E-01	.34E-02	4.112
.723	.458E-01	.22E-02	4.259
.773	.293E-01	.15E-02	4.404
.823	.183E-01	.10E-02	4.545
.874	.114E-01	.68E-03	4.683
.924	.691E-02	.47E-03	4.816
.973	.355E-02	.29E-03	4.942
1.038	.197E-02	.15E-03	5.104
1.140	.679E-03	.86E-04	5.349
1.239	.263E-03	.53E-04	5.577
1.347	.599E-04	.26E-04	5.815
1.433	.301E-04	.23E-04	5.998
1.554	.212E-04	.17E-04	6.246
1.658	.113E-04	.12E-04	6.452
1.784	.511E-04	.22E-04	6.693
1.922	.427E-04	.16E-04	6.948
2.080	.432E-04	.13E-04	7.228
2.289	.352E-04	.12E-04	7.583
2.591	.192E-04	.60E-05	8.068
2.951	.169E-04	.56E-05	8.612
3.328	.217E-05	.15E-05	9.146

TABLE VI. P_{LAB} = 300-340 GeV/c, s_{ave} = 602 GeV^2
(σ_T = 40.1 mb, P* = 12.2 GeV/c)

t_{ave}	dσ/dt	Error	θ*
	mb/$(GeV/c)^2$		deg.
.151	.136E+02	.62E+00	1.820
.174	.108E+02	.45E+00	1.956
.204	.743E+01	.32E+00	2.118
.239	.527E+01	.22E+00	2.290
.279	.335E+01	.15E+00	2.472
.323	.207E+01	.92E-01	2.662
.373	.123E+01	.58E-01	2.861
.423	.747E+00	.38E-01	3.047
.474	.457E+00	.26E-01	3.224
.524	.276E+00	.18E-01	3.391
.577	.195E+00	.87E-02	3.557
.624	.117E+00	.52E-02	3.700
.674	.731E-01	.33E-02	3.846
.723	.454E-01	.21E-02	3.983
.775	.284E-01	.14E-02	4.124
.824	.173E-01	.92E-03	4.253
.873	.113E-01	.65E-03	4.377
.923	.700E-02	.45E-03	4.501
.971	.439E-02	.32E-03	4.617
1.041	.203E-02	.15E-03	4.780
1.141	.817E-03	.89E-04	5.005
1.241	.165E-03	.37E-04	5.220
1.343	.699E-04	.29E-04	5.430
1.434	.194E-04	.15E-04	5.611
1.551	.334E-04	.26E-04	5.836
1.671	.241E-04	.21E-04	6.057
1.780	.364E-04	.19E-04	6.252
1.918	.462E-04	.15E-04	6.490
2.095	.403E-04	.12E-04	6.783
2.277	.329E-04	.10E-04	7.072
2.588	.146E-04	.50E-05	7.540
3.086	.157E-04	.50E-05	8.235
3.479	.445E-05	.23E-05	8.745

TABLE VII. P_{LAB} = 340-400 GeV/c, s_{ave} = 677 GeV^2

(σ_T = 40.3 mb, P* = 13.0 GeV/c)

t_{ave}	dσ/dt mb/(GeV/c)^2	Error	θ* deg.
.175	.115E+02	.52E+00	1.847
.205	.829E+01	.36E+00	1.999
.239	.588E+01	.25E+00	2.159
.279	.378E+01	.17E+00	2.332
.322	.234E+01	.11E+00	2.506
.372	.143E+01	.68E-01	2.693
.423	.847E+00	.45E-01	2.872
.473	.512E+00	.30E-01	3.036
.524	.293E+00	.15E-01	3.196
.572	.178E+00	.11E-01	3.341
.623	.116E+00	.78E-02	3.485
.672	.755E-01	.59E-02	3.619
.724	.398E-01	.19E-02	3.757
.773	.258E-01	.13E-02	3.882
.824	.150E-01	.81E-03	4.009
.873	.101E-01	.59E-03	4.126
.924	.667E-02	.42E-03	4.245
.973	.418E-02	.30E-03	4.356
1.041	.175E-02	.13E-03	4.506
1.144	.603E-03	.72E-04	4.724
1.241	.182E-03	.40E-04	4.920
1.346	.530E-04	.24E-04	5.124
1.414	.882E-05	.99E-05	5.252
1.550	.254E-04	.18E-04	5.499
1.651	.302E-04	.16E-04	5.676
1.774	.256E-04	.12E-04	5.883
1.920	.480E-04	.15E-04	6.121
2.079	.474E-04	.12E-04	6.369
2.327	.338E-04	.11E-04	6.739
2.549	.136E-04	.48E-05	7.054
3.012	.936E-05	.38E-05	7.668
3.662	.604E-05	.28E-05	8.457

FIGURE CAPTIONS

1. Schematic layout of the experimental apparatus. The inset shows the neutron detector in more detail.
2. χ^2 distributions for the fitted events with (a) $0.4 \leq -t \leq 0.8$ $(GeV/c)^2$ and (b) $1.3 \leq -t \leq 1.6$ $(GeV/c)^2$. The solid curve represents the expected distribution for a two-constraint fit.
3. The geometric detection efficiency for the low $|t|$ (Pos. I) and high $|t|$ (Pos. II) data at 200 GeV/c. At 100 GeV/c (dotted line) the neutron detector limits the acceptance at large $|t|$.
4. Experimental resolution of the data: (a) the uncertainty in the four-momentum transfer squared; and (b) the fractional uncertainty in the incident neutron momentum for several values of the four-momentum transfer squared.
5. Neutron-proton elastic differential cross sections from 70 to 400 GeV/c as measured by this experiment.
6. Logarithmic slope parameter evaluated at $-t = 0.2$ $(GeV/c)^2$ for neutron-proton and proton-proton elastic scattering. The solid curve is the prediction of Kane and Seidl(12).
7. Comparison of neutron-proton elastic differential cross sections from this experiment and proton-proton elastic differential cross sections from Akerlof <u>et al</u>.,[6] and Bomberowitz <u>et al</u>.,[13] at 200 GeV/c.
8. Neutron-proton differential cross sections for 75-125 GeV/c, 175-225 GeV/c and 265-300 GeV/c bins. Also shown are the 200 GeV/c proton-proton data of Akerlof <u>et al</u>., (6) preliminary data form Bomberowitz <u>et al</u>., (12) and the 280 GeV/c p-p data of Kwak <u>et al</u>. (14).

9. Difference between neutron-proton and proton-proton elastic differential cross sections plotted against s for $-t = 1.25$ $(GeV/c)^2$.

10. Composite of neutron-proton elastic differential cross sections for this experiment, Stone _et al._ (3) and Bohmer _et al._ (9). The number in parentheses gives the incident momentum.

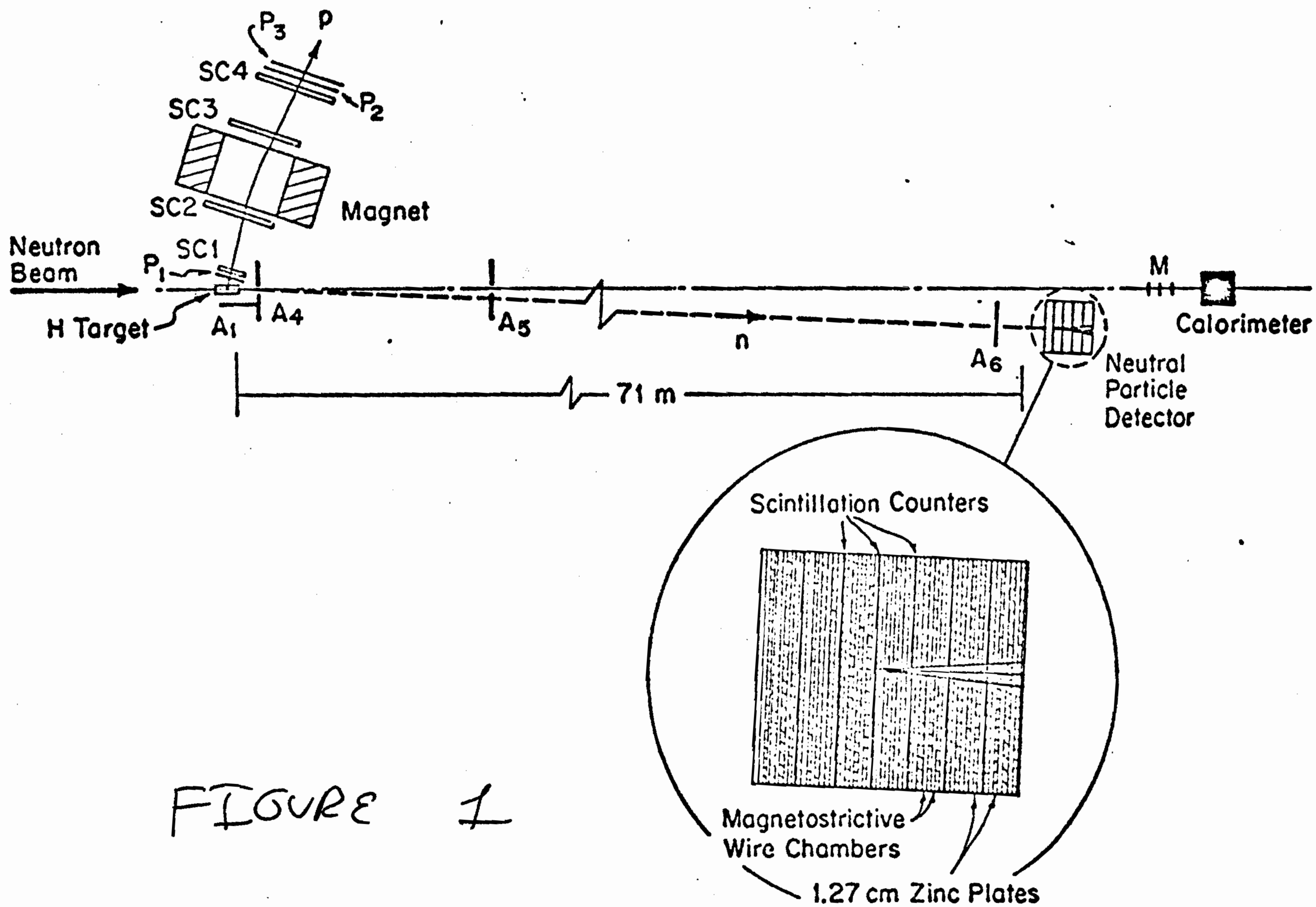
P3
p
SC4
P2
SC3
SC2
Magnet
Neutron Beam
SC1
P1
H Target
A1
A4
A5
n
A6
M
Calorimeter
Neutral Particle Detector
71 m
Scintillation Counters
Magnetostrictive Wire Chambers
1.27 cm Zinc Plates

FIGURE 1

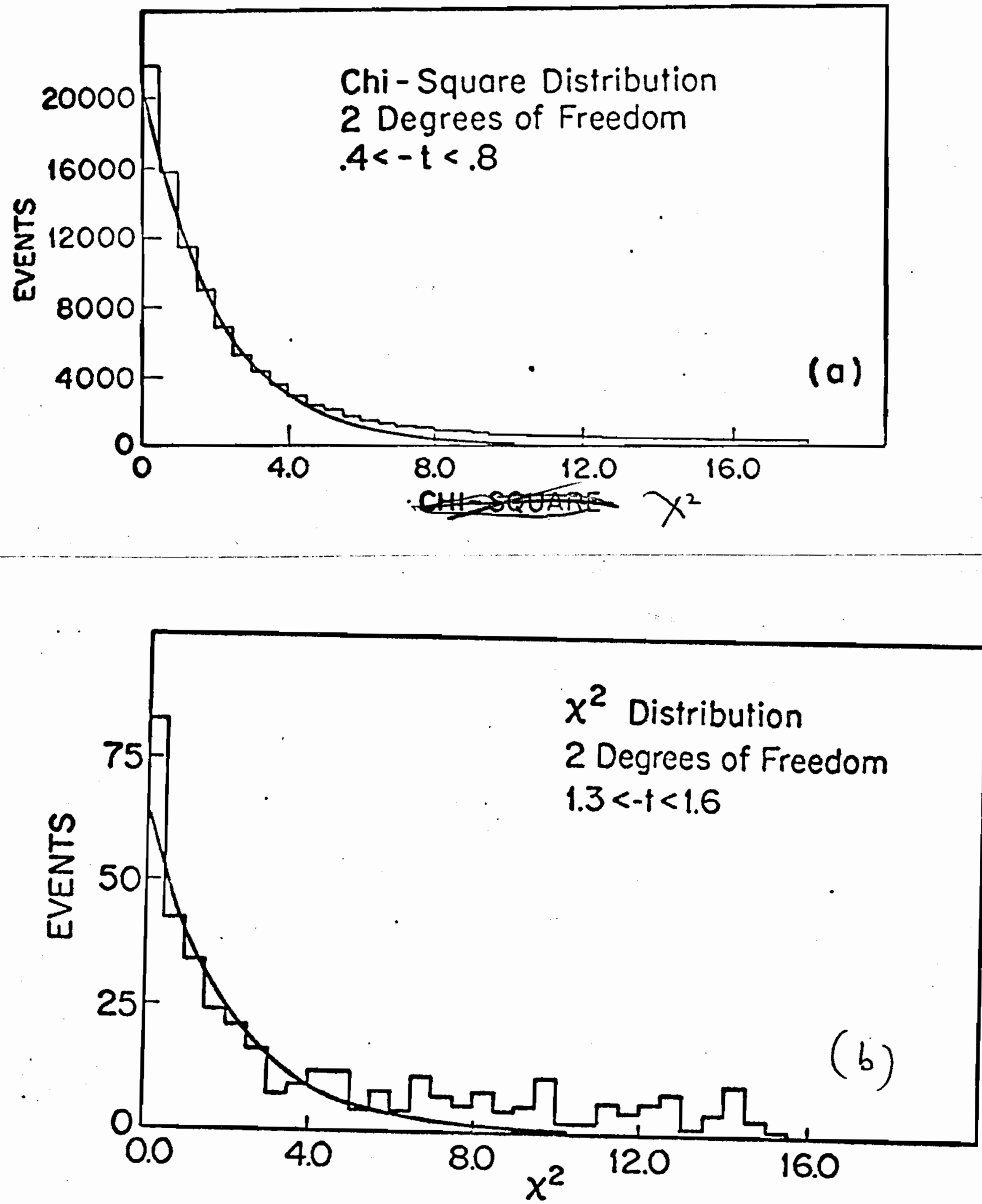
Chi-Square Distribution
2 Degrees of Freedom
.4< -t < .8
20000
16000
12000
8000
4000
0
EVENTS
(a)
0
4.0
8.0
12.0
16.0
CHI-SQUARE
χ^2
χ^2 Distribution
2 Degrees of Freedom
1.3<-t<1.6
75
50
25
0
EVENTS
(b)
0.0
4.0
8.0
12.0
16.0
χ^2

FIGURE 2

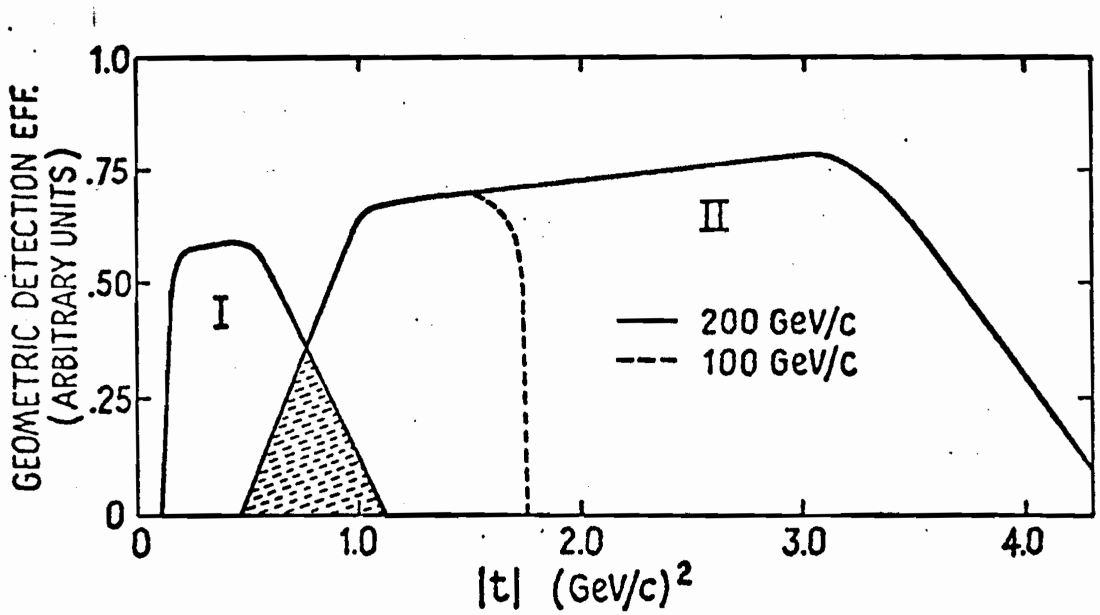
GEOMETRIC DETECTION EFF.
(ARBITRARY UNITS)
1.0
.75
.50
.25
0
0
1.0
2.0
3.0
4.0
|t| (GeV/c)²
I
II
200 GeV/c
100 GeV/c

Figure 3.

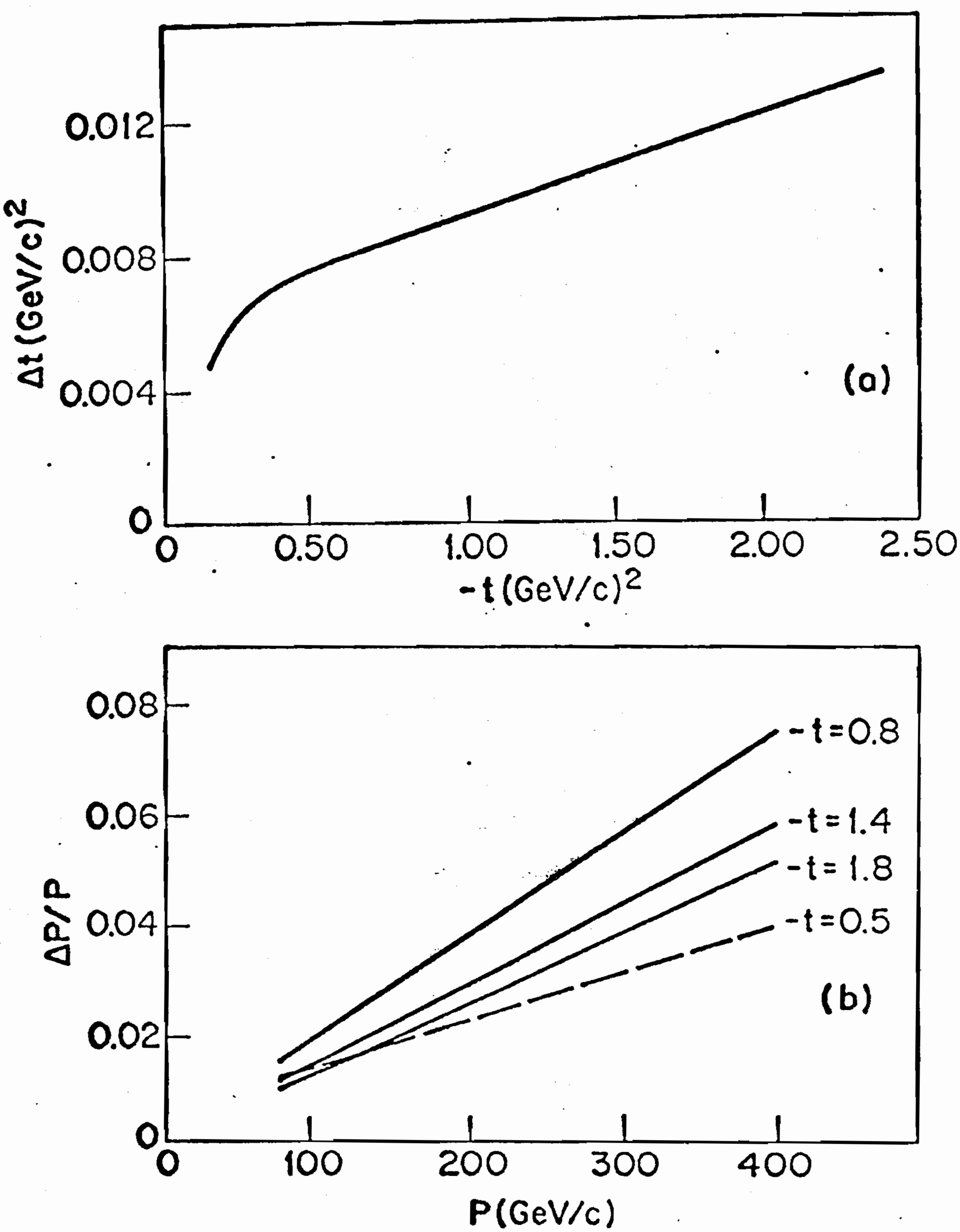
0.012
0.008
0.004
0
$\Delta t\,(GeV/c)^2$
(a)
0
0.50
1.00
1.50
2.00
2.50
$-t\,(GeV/c)^2$
0.08
0.06
0.04
0.02
0
ΔP/P
$-t = 0.8$
$-t = 1.4$
$-t = 1.8$
$-t = 0.5$
(b)
0
100
200
300
400
P(GeV/c)

FIGURE 4

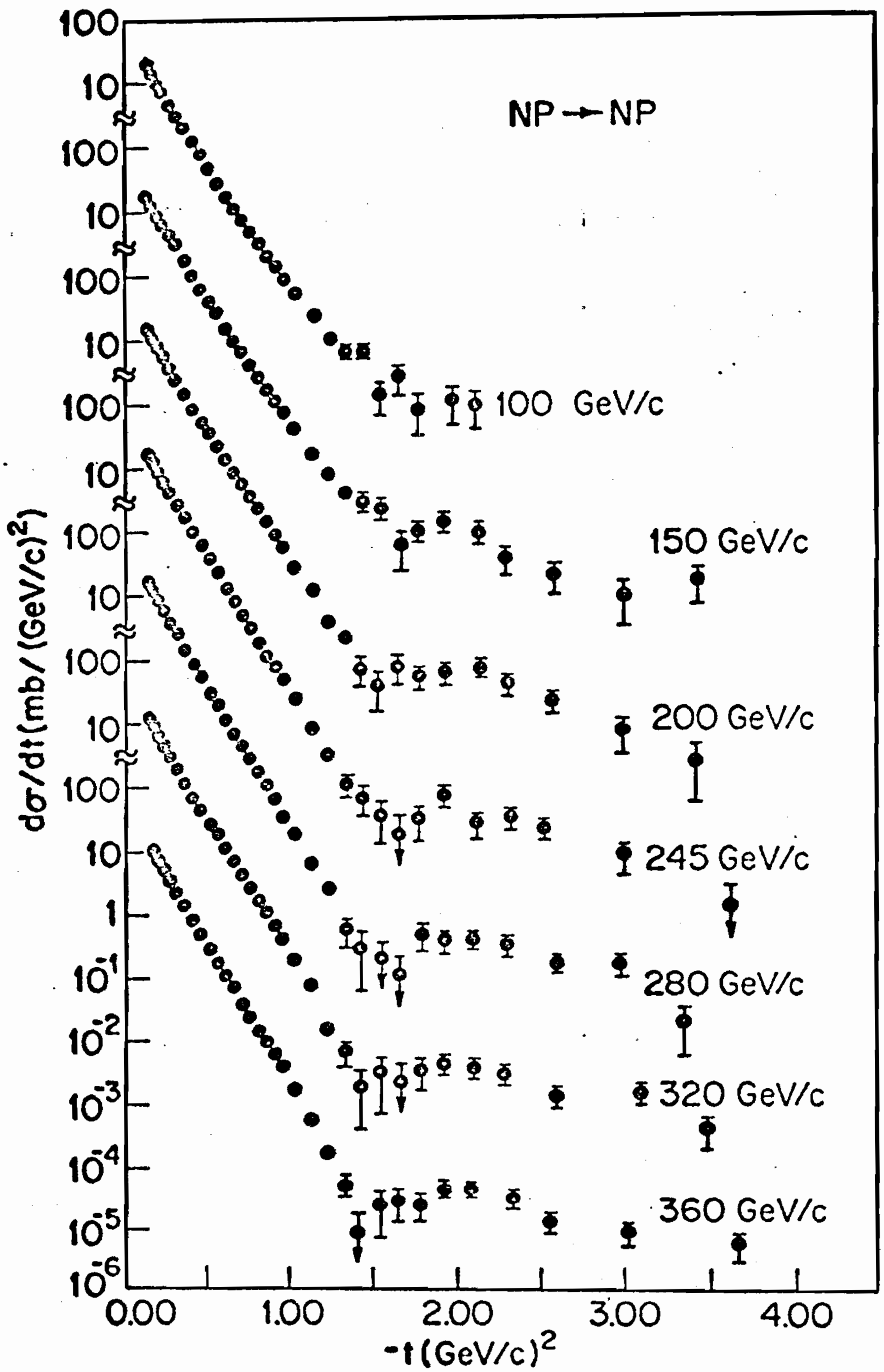
NP → NP
100
10
100
10
100
10
100
10
100
10
100
10
100
10
1
10^{-1}
10^{-2}
10^{-3}
10^{-4}
10^{-5}
10^{-6}
dσ/dt (mb/(GeV/c)²)
100 GeV/c
150 GeV/c
200 GeV/c
245 GeV/c
280 GeV/c
320 GeV/c
360 GeV/c
0.00
1.00
2.00
3.00
4.00
-t (GeV/c)²

FIGURE 5

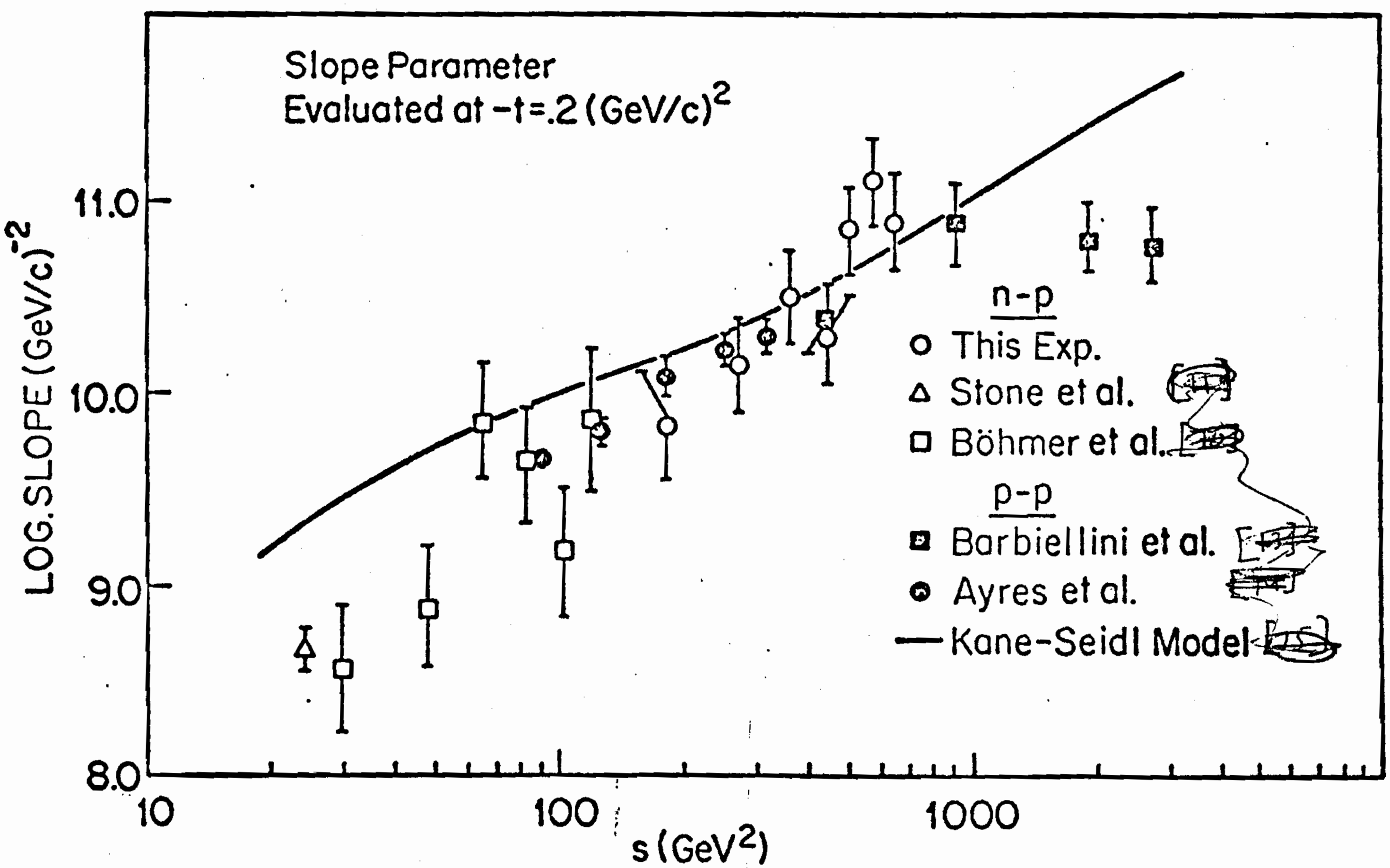

Slope Parameter
Evaluated at −t=.2 (GeV/c)^2
LOG. SLOPE (GeV/c)$^{-2}$
11.0
10.0
9.0
8.0
10
100
1000
s (GeV^2)
n−p
This Exp.
Stone et al.
Böhmer et al.
p−p
Barbiellini et al.
Ayres et al.
Kane−Seidl Model

FIGURE 6

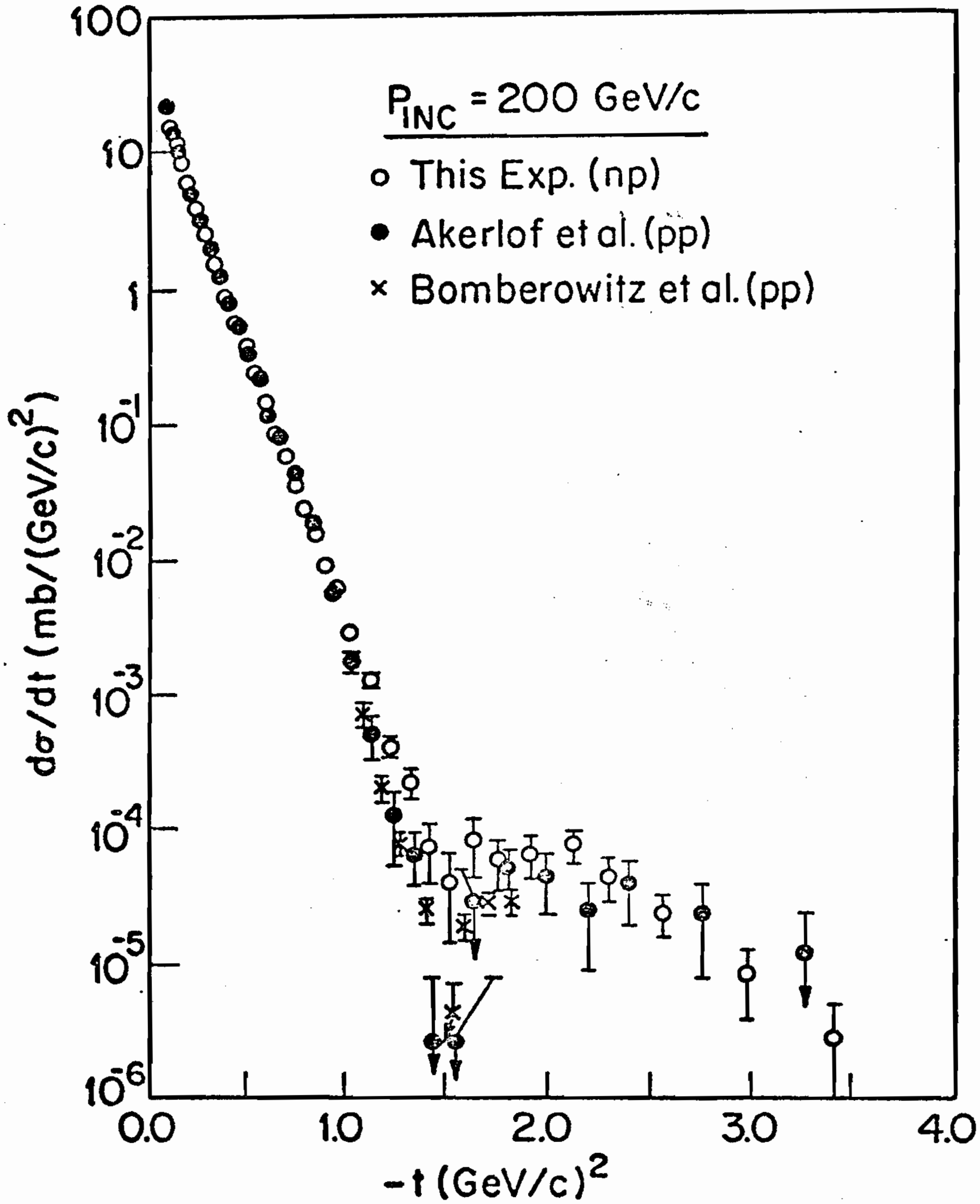

100
10
1
10^{-1}
10^{-2}
10^{-3}
10^{-4}
10^{-5}
10^{-6}
$d\sigma/dt$ (mb/(GeV/c)^2)
P_{INC} = 200 GeV/c
o This Exp. (np)
● Akerlof et al. (pp)
× Bomberowitz et al. (pp)
0.0
1.0
2.0
3.0
4.0
$-t$ (GeV/c)^2

FIGURE 7

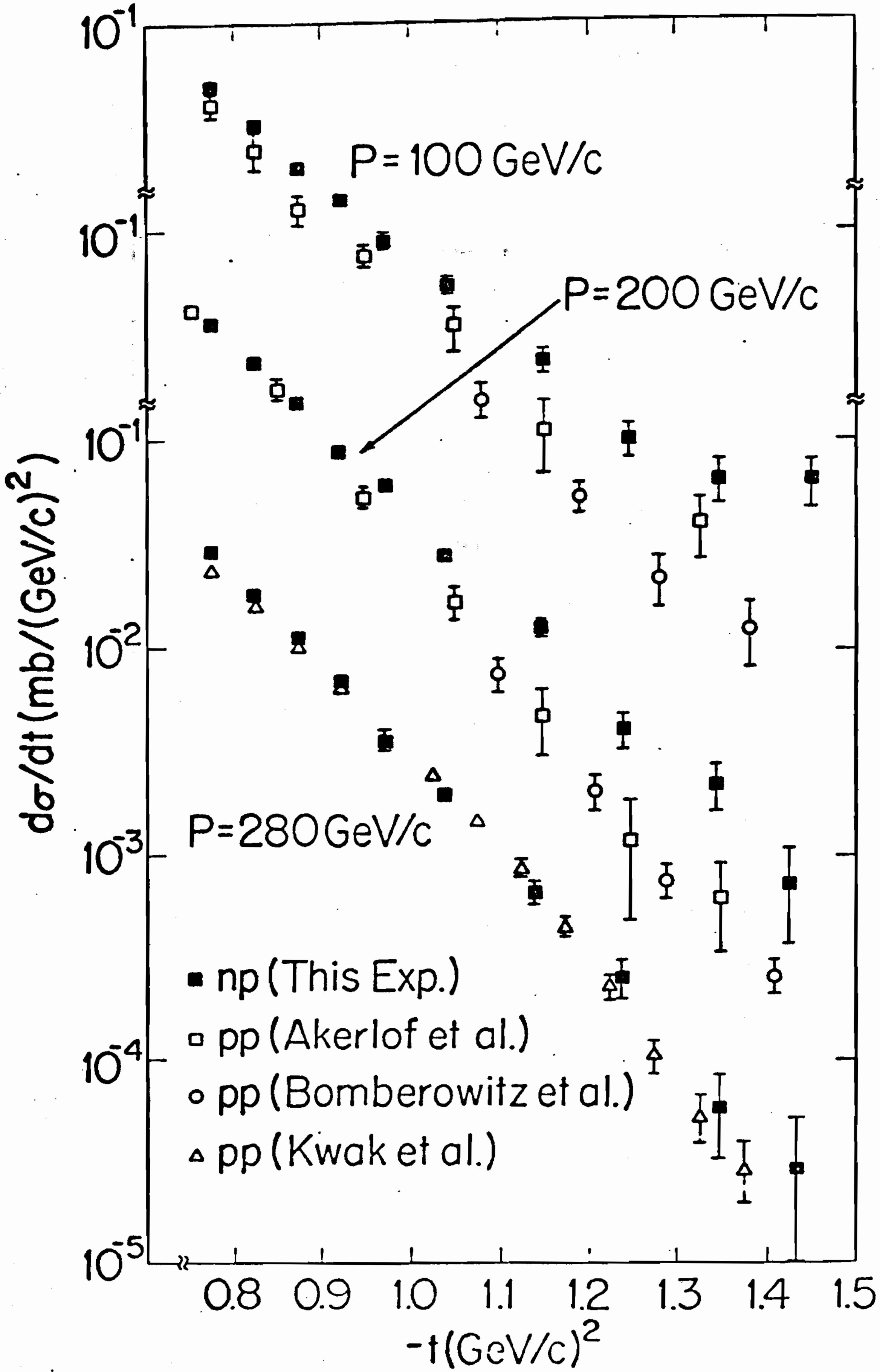

P = 100 GeV/c
P = 200 GeV/c
P = 280 GeV/c
np (This Exp.)
pp (Akerlof et al.)
pp (Bomberowitz et al.)
pp (Kwak et al.)
dσ/dt (mb/(GeV/c)²)
-t (GeV/c)²
10⁻¹
10⁻¹
10⁻¹
10⁻²
10⁻³
10⁻⁴
10⁻⁵
0.8
0.9
1.0
1.1
1.2
1.3
1.4
1.5

FIGURE 8

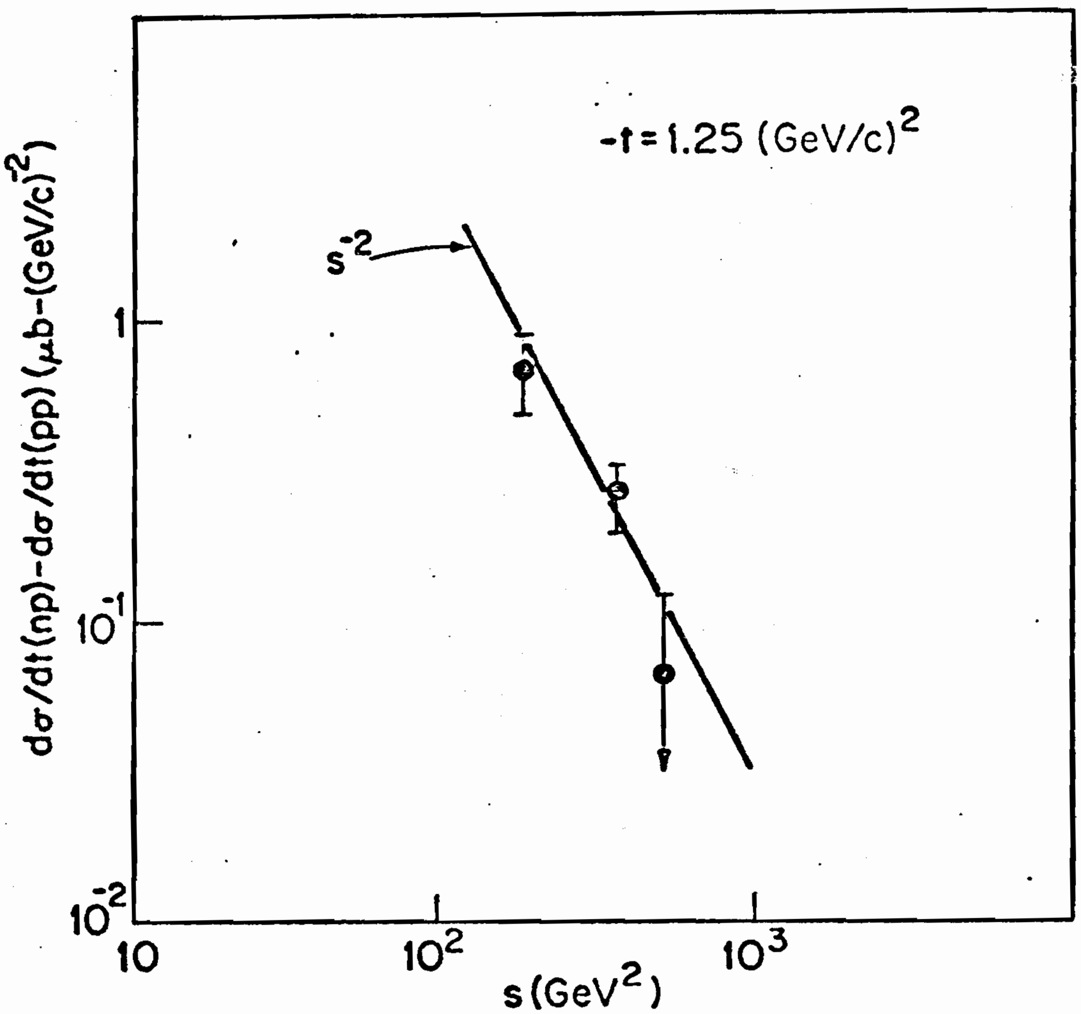
-t = 1.25 (GeV/c)^2
s^{-2}
dσ/dt(np) − dσ/dt(pp) (μb-(GeV/c)$^{-2}$)
1
10^{-1}
10^{-2}
10
10^2
10^3
s (GeV^2)

FIGURE 9

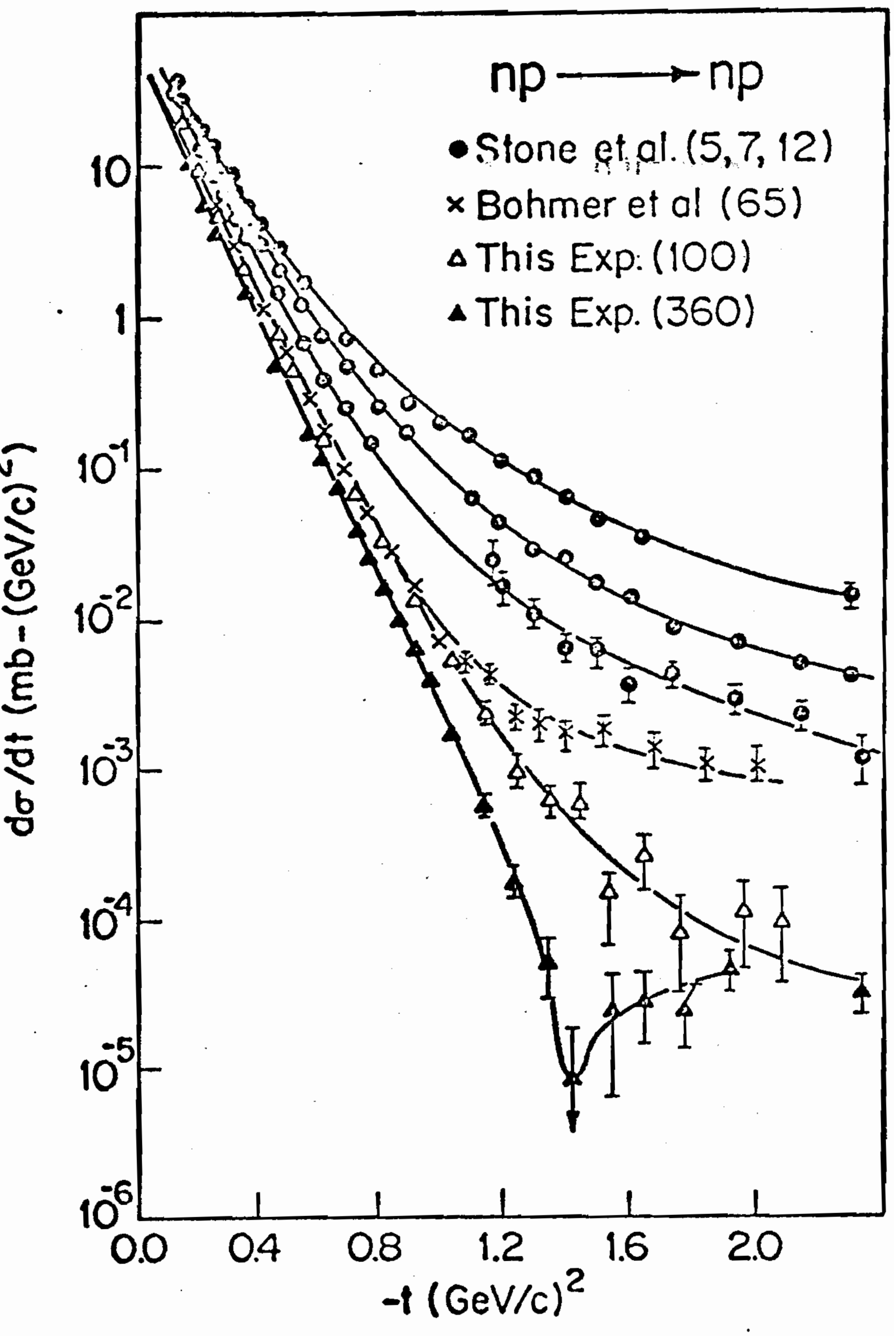

np → np
● Stone et al. (5, 7, 12)
× Bohmer et al (65)
△ This Exp. (100)
▲ This Exp. (360)
dσ/dt (mb-(GeV/c)^-2)
10
1
10^-1
10^-2
10^-3
10^-4
10^-5
10^-6
0.0
0.4
0.8
1.2
1.6
2.0
-t (GeV/c)^2

FIGURE 10